Earth, Planets and Space
a SpringerOpen Journal

LETTER Open Access

# Electrical conductivity of brine-bearing quartzite at 1 GPa: implications for fluid content and salinity of the crust

Akira Shimojuku[1,2*], Takashi Yoshino[1] and Daisuke Yamazaki[1]

**Abstract**

The electrical conductivity of brine-bearing quartzite with fluid fractions of 0.19 to 0.30 and salinity of 3 to 17 wt.% was measured at 800 to 1,100 K and 1 GPa. The conductivity of the brine-bearing quartzite increases with salinity and fluid fraction, but is almost independent of temperature. Our results suggest that regions of high conductivity ($10^{-3}$ to $10^{-2}$ S/m) in the crust could be explained by the presence of quartzite with fluids of salinity similar to that of seawater. To account for those regions with the highest conductivity of $10^{-1}$ S/m, quartzite with fluid of high salinity (>10 wt.%) is required.

**Keywords:** Electrical conductivity; Fluid; Brine; High-conductivity anomaly

## Correspondence/Findings

### Introduction

Recent magnetotelluric surveys have revealed that there are regions with anomalously high electrical conductivity in the middle to the lower crust (e.g., Ogawa et al. 2001; Wannamaker et al. 2009). The conductivity of these regions ranges from $10^{-3}$ to $10^{-1}$ S/m, which is at least 1 to 2 orders of magnitude higher than the conductivity of dry crustal rocks (e.g., Olhoeft 1981; Marquis and Hyndman 1992). Several explanations for this high conductivity have been suggested, which include the presence of interconnected graphite (e.g., Duba and Shankland 1982; Frost et al. 1989), aqueous fluids (e.g., Hyndman and Hyndman 1968; Hyndman and Shearer 1989; Glover and Vine 1994), partial melts (e.g., Hermance 1979; Wannamaker 1986; Gaillard et al. 2004), sulfides (e.g., Ducea and Park 2000), and magnetite (Stesky and Brace 1973).

Of these, the presence of aqueous fluids has been considered the most plausible candidate (e.g., Marquis and Hyndman 1992; Glover and Vine 1994). However, Shimojuku et al. (2012) demonstrated that the electrical conductivity of fluid-bearing quartzite under deep crustal conditions was definitely lower than that of the high-conductivity anomalies, even when the quartzite contained a large fluid fraction (0.32). This suggests that other dissolved species such as $Na^+$, $Cl^-$, and $Al^{3+}$ are required in the fluids to account for the high-conductivity anomalies. NaCl is commonly found in fluid inclusions in rocks from the lower crust (e.g., Banks et al. 1991). In addition, the high-conductivity anomalies observed in the crust above the subducting plate are closely related to active faults (e.g., Wannamaker et al. 2009). Thus, it is important to measure the electrical conductivity of brine-bearing rocks. Glover and Vine (1994) reported on the electrical conductivity of brine-bearing rocks at 0.2 GPa. However, their measurement is limited to a salinity of approximately 3 wt.%. In addition, the exact fluid fraction of their recovered samples was unclear. Thus, it is impossible to constrain the plausible fluid fraction and salinity in the crust from their data set.

In the present study, we measure the electrical conductivity of brine-bearing quartzite as a function of salinity and fluid fraction at 1 GPa and 800 to 1,100 K and discuss the salinity and fluid fractions needed to realize the crustal high-conductivity anomalies. Although natural lower crustal rocks are composed of granulite, gabbro, and amphibolite, we used quartzite as a simplified analogue for the crustal rocks in order to focus on the

* Correspondence: simojuku@eri.u-tokyo.ac.jp
[1]Institute for Study of the Earth's Interior, Okayama University, Misasa, Tottori 682-0193, Japan
[2]Earthquake Research Institute, University of Tokyo, 1-1-1 Yayoi, Bunkyo-ku, Tokyo 113-0032, Japan

effects of the salinity and fluid fraction on the bulk conductivity.

## Experimental procedures

High-pressure and high-temperature experiments were performed using the DIA-type apparatus installed at the Institute for Study of the Earth's Interior, Okayama University. The cell assembly was identical to that used by Shimojuku et al. (2012). It should be noted that we used a cylindrical sleeve of single crystal quartz as a capsule, which effectively prevents water loss from the sample during the conductivity measurements (Shimojuku et al. 2012).

The starting materials were prepared by mixing the reagents $SiO_2$, $SiO_2{\cdot}nH_2O$, and NaCl powders. By changing the mixing ratio, we produced four types of starting material. Because the $n$ value of the $SiO_2{\cdot}nH_2O$ powder can differ on a daily basis, the exact water contents of the starting materials are unclear. Thus, the fluid fraction (water content) of the samples was calculated from the recovered samples by counting the areal fraction of pores in the secondary electron image (SEI) using ImageJ software. First, the area of fluid and quartz in the SEI was distinguished by setting the function 'Threshold' in ImageJ. In this function, the gray-scale image was converted into a binary image with only two values: 0 for white (quartz), and 255 for black (fluid). Then, the volume fraction of the fluid was calculated based on the ratio between the total and fluid areas using the function 'Measure' in ImageJ. The number of analyzed SEIs was at least 15 for each sample. The average fluid fraction was adopted, and the uncertainty was $1\sigma$ from the averaged value.

The SEIs were obtained with a field-emission scanning electron microscope (FE-SEM, JEOL JSM-7001 F, Tokyo, Japan) operated at an accelerating voltage of 15 kV and a current of 12 nA. Salinity was estimated from the weight ratio of the amount of fluid determined from the porosity in the SEI and the amount of NaCl powder added to the starting material, based on the assumption that fluid did not escape during the conductivity measurements. This is deemed reasonable because the capsule of the single crystal quartz effectively prevents water loss from the sample (Shimojuku et al. 2012). The uncertainties of salinity are estimated by propagating the uncertainties of the amount of fluid.

The electrical resistance of the sample was measured by an impedance gain-phase analyzer combined with a Solartron 1296 interface with amplitude of 1 V and frequency range of $10^{-1}$ to $10^{6}$ Hz. The electrical conductivity $\sigma$ (S/m) was derived directly from the equation $\sigma = l/SR$, where $l$ is the length of the sample (m), $S$ is a cross-sectional area of the sample ($m^2$), and $R$ is the resistance of the sample ($\Omega$).

First, the sample was pressurized to 1 GPa at room temperature, and the electrical conductivity was measured at elevated temperatures of 300, 600, 900, and 1,100 K (the heating path). The sample was then held at 1,100 K for at least 12 h to reach textural equilibrium. Then, conductivity was measured at intervals of 25 K as the temperature fell to 800 K (the cooling path). The sample was rapidly reheated to 1,100 K to confirm the reproducibility of the conductivity at 1,100 K. Finally, the sample was quenched from 1,100 K by shutting off the power supply to the heater. The recovered samples were quickly covered by epoxy and placed into a heater under vacuum to solidify the epoxy. Subsequently, the sample was prepared as a polished section for FE-SEM analysis.

## Results

Typical SEIs of the recovered samples with the nominal fluid fractions of 0.19 (run A2354) and 0.29 (run A2343) are shown in Figure 1a,b. The fluid portions are

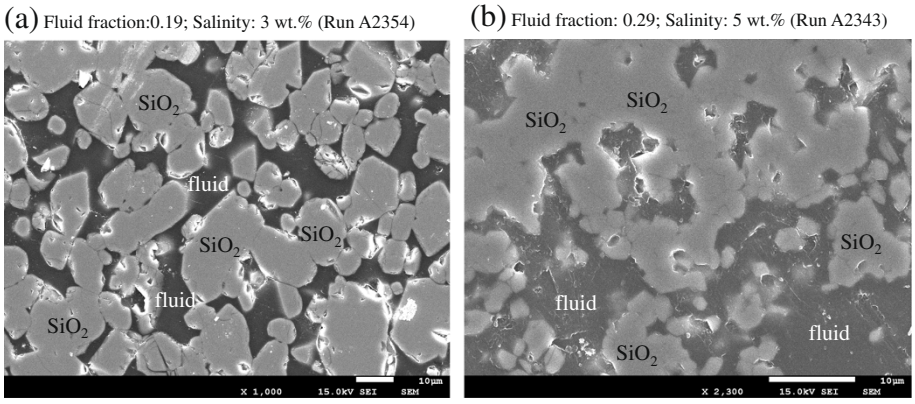


**Figure 1 Representative SEIs of recovered samples. (a)** Run A2354 with fluid fraction of 0.19 and salinity of 3 wt.%. **(b)** Run A2343 with fluid fraction of 0.29 and salinity of 5 wt.%. The dark-gray and light-gray regions correspond to the fluid portions (filled with epoxy) and quartz, respectively.

observed as pores filled with epoxy resin, which are located along grain boundaries or at grain corners. Some pores at the grain corners are present as large pools. Fluid fractions and salinity ranged from 0.19 to 0.30 and 3 to 17 wt.%, respectively (Table 1).

Typical Cole-Cole plots for the samples with fluid fractions of 0.19 (run A2354) and 0.30 (run A2341) are shown in Figure 2a,b. Also shown are the equivalent circuits (*R*-*C* parallel circuit) expected from the obtained impedance spectra. All the impedance spectra are composed of a semicircle and an additional tail at low frequencies (Figure 2). Roberts and Tyburczy (1999) deduced that the electrical circuit was different in terms of the connectivity of partial melts in the rock. In the case of the presence of an interconnected melt pathway, the circuit was composed of the response of the grain interior and basaltic melts in a parallel circuit. On the other hand, in the absence of an interconnected melt pathway, the circuit was composed of the response of the grain interior and the basaltic melt in a series circuit. Thus, it was expected that the impedance spectra of a single semicircle would be obtained when the fluid phase forms an interconnecting network, as observed in Shimojuku et al. (2012), because the resistivity of the grain interior (Yoshino and Noritake 2011) is at least 3 orders of magnitude higher than that of the interconnecting fluid phase at 800 to 1,100 K. Thus, the presence of the single semicircle would indicate that the fluid establishes interconnection and that the semicircular shape is controlled by ionic conduction in the interconnected fluids. The low-frequency tail is probably due to electrode-sample interface effects (e.g., ten Grotenhuis et al. 2005). The slope with 45° can be interpreted as Warburg impedance, which occurs via diffusion of charge species near the electrode interface.

Caricchi et al. (2011) obtained impedance spectra comprising two semicircles in melt-bearing olivine aggregates. They discussed that high-frequency and low-frequency arcs were responsible for melt pockets and interconnected melt in long-range scales, respectively. In the present study, we could not obtain the two semicircles as observed in Caricchi et al. (2011). This suggests that the volume fraction of isolated fluid pockets is negligibly small.

**Table 1 Fluid fraction and salinity of the samples**

| Run | Fluid fraction | Salinity[a] (wt.%) |
|---|---|---|
| A2354 | 0.19 (0.05) | 3 (1) |
| A2359 | 0.19 (0.03) | 10 (2) |
| A2343 | 0.29 (0.03) | 5 (1) |
| A2341 | 0.30 (0.04) | 17 (2) |

Numbers in parentheses represent the uncertainties. [a]The values with respect to the water content.

The resistivity of the brine-bearing quartzite was determined by fitting the semicircular part of the impedance data, excluding the low-frequency tail. The size and shape of the semicircle were very similar at 900 and 1,100 K (Figure 2a,b). This indicates that the conductivity of brine-bearing quartzite is not strongly dependent on temperature. Uncertainties that arose from the fitting process led to an uncertainty of ±0.03 log units in the electrical conductivity values.

The dihedral angle of the $SiO_2$-$H_2O$-NaCl system was reported to be less than 60° at 1 GPa and 1,273 K (Watson and Brenan 1987). This small value of dihedral angle is further evidence that the fluid forms an interconnected network along grain boundaries in the quartz aggregates.

Figure 3 shows variations in the electrical conductivity of brine-bearing quartzite (runs A2343 and A2354) during the heating and cooling paths as a function of reciprocal temperature. The conductivity data in the heating path are scattered (Figure 3). This is because the conductivity was affected by absorbed water in the specimen assembly (e.g., Yoshino 2010). Therefore, we did not use the conductivity data obtained in the heating path. During the heating path, $SiO_2 \cdot nH_2O$ would dehydrate and then NaCl would dissolve into the fluid. After reaching 1,100 K, the sample was held for at least 12 h to reach textural equilibrium. The conductivity decreased by 0.02 to 0.7 orders of magnitude and reached a constant value during this period (Figure 3). This indicates that the absorbed water in the specimen assembly was completely purged and that the samples reached textural equilibrium. Then, the conductivity was measured at intervals of 25 K as the temperature fell to 800 K. The sample was rapidly reheated to 1,100 K to confirm the reproducibility of the conductivity at 1,100 K (Figure 3). The similar conductivity values indicate that both the fluid fraction and salinity maintain constant values. The conductivity values obtained from the cooling path were adopted for the analysis.

Figure 4 shows the temperature effect on electrical conductivity of brine-bearing quartzite obtained from the cooling path. The conductivity is nearly constant at temperatures of 800 to 1,100 K, and it increases with both the fluid fraction and salinity. The conductivity of the NaCl-free fluid-bearing quartzite (Shimojuku et al. 2012) is 1 and 2 orders of magnitude lower than that of the brine-bearing quartzite with salinities of 5 and 17 wt.%, respectively, in similar fluid fractions (0.29 to 0.32). This indicates that the presence of NaCl in fluids strongly increases the conductivity. The α-quartz to β-quartz transition occurs at about 1,073 K at 1 GPa (e.g., Ostrovsky 1967). Because we did not observe a change or jump of conductivity in this condition, the transition might not affect the fluid fraction and salinity.

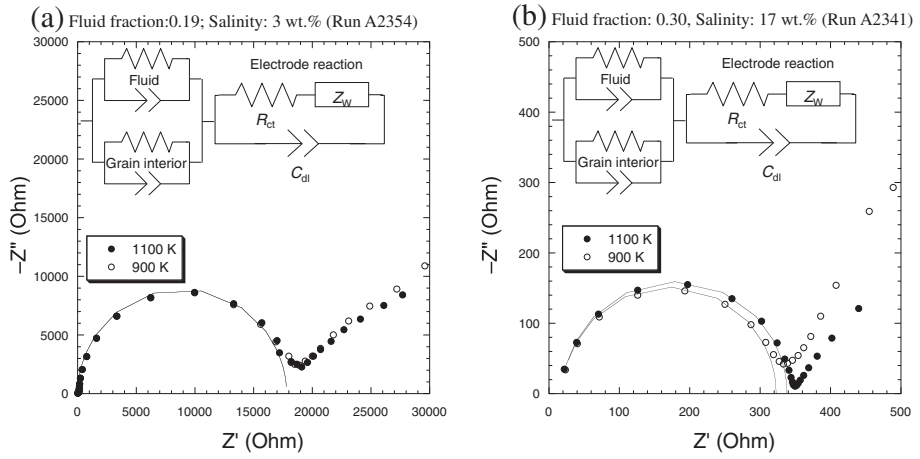


**Figure 2 Representative impedance spectra. (a)** Run A2354 with fluid fraction of 0.19 and salinity of 3 wt.%. **(b)** Run A2341 with fluid fraction of 0.30 and salinity of 17 wt.%. The straight segments indicate the lines fitted to the data points. The insets show the expected circuit. The low-frequency tail is possibly approximated by Randles circuit (Randles 1947), which includes a double-layer capacitor ($C_{dl}$), charge transfer reaction resistance ($R_{ct}$), and Warburg impedance ($Z_W$).

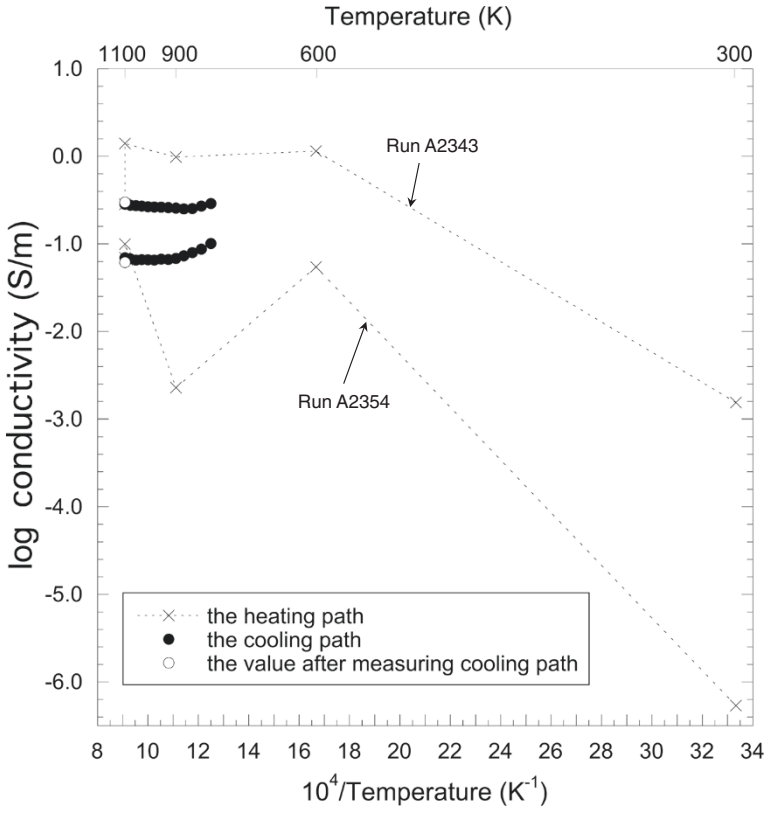


**Figure 3 Variation of the electrical conductivity during the heating path (crosses) and cooling path (solid circles).** After completing the measurements of the cooling path, the sample was reheated to 1,100 K. Then, we measured the conductivity again (open circles) to confirm the reproducibility.

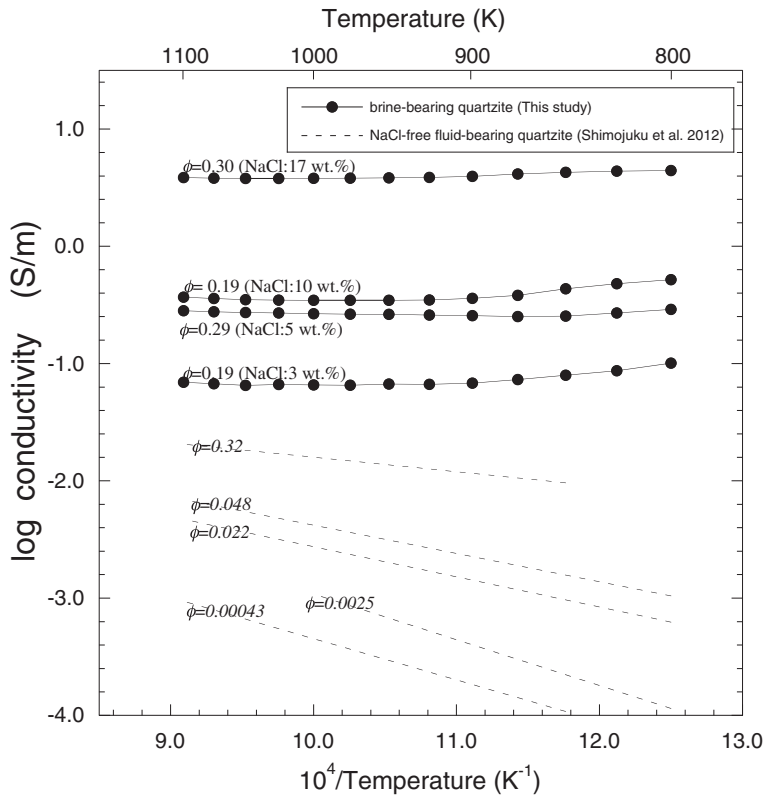


**Figure 4 Arrhenius plots of electrical conductivity for brine-bearing quartzite at 1 GPa (solid circles).** The solid lines show the smoothed fit to the data points. The attached numbers indicate the fluid fractions ($\varphi$) and salinity. The dashed lines indicate the electrical conductivity of NaCl-free fluid-bearing quartzite measured by Shimojuku et al. (2012) with fluid fractions shown in italics.

## Discussion

The main charge carriers for the electrical conduction in the brine-bearing quartzite are $Na^+$, $Cl^-$, and soluble ionic species derived from $SiO_2$. As $SiO_2$ dissolves into fluid mainly as neutral hydroxide of $Si(OH)_4$ (e.g., Wasserburg 1958; Wood 1958), the majority of the charge carriers are $Na^+$ and $Cl^-$ ions. The conductivity of the NaCl-free fluid-bearing quartzite increases with temperature, whereas that of the brine-bearing quartzite is nearly constant with temperature (Figure 4). This indicates that the concentrations of $Na^+$ and $Cl^-$ ions in the fluid are almost constant over the measured temperature ranges. This is reasonable because NaCl dissolves into the aqueous fluid irrespective of temperature.

Nesbitt (1993) reported on the variation of the resistivities of KCl solution with salinities of 3.6, 13.5, and 24.7 wt.% at 0.1 to 0.3 GPa and 273 to 773 K. The results indicated that resistivity was almost constant from 473 to 773 K at salinities of 13.5 and 24.7 wt.%. The temperature insensitivity was explained by the constancy of the mobility of ions (Nesbitt 1993). Although temperature insensitivity was not clearly observed in the salinity of 3.6 wt.% in Nesbitt (1993), our data showed that resistivity was almost constant, even in the low salinity of 3 wt.%. Because our experimental pressure and temperature conditions were higher than those in Nesbitt (1993), the mobility of Na and Cl ions in aqueous fluid might be insensitive to temperature under high-pressure and high-temperature conditions.

The electrical conductivity of rocks generally increases with the increasing volume fraction of melt and/or fluid phases, which have a constant number of charge carriers (e.g., ten Grotenhuis et al. 2005; Yoshino et al. 2010; Shimojuku et al. 2012). In order to evaluate the effect of fluid fraction on the bulk electrical conductivity, various geometrical models have been proposed, such as the Hashin-Shtrikman upper and lower bound models (Hashin and Shtrikman 1962), the cube model (Waff 1974), and the tube model (Schmeling 1986).

The Hashin-Shtrikman upper bound (HS+) and cube models are applicable to cases in which fluid is distributed along the grain boundaries and triple junctions. The difference between the two models relates to whether the shape of the resistive phase is spherical or square. The two models usually yield similar values of bulk conductivity (e.g., ten Grotenhuis et al. 2005). The tube model describes cases in which fluid is not distributed along the grain boundaries, but in a network along

the triple junctions. The Hashin-Shtrikman lower bound model addresses cases in which fluid is present as isolated pockets and does not form an interconnected network.

The microstructure and shape of the impedance spectra demonstrated that the fluid phase was interconnected. Thus, the interconnected HS + and cube models are the most appropriate for reproducing the texture of the brine-bearing quartzite. In the HS + model, the bulk conductivity of fluid-bearing rocks ($\sigma_b$) is expressed as (Hashin and Shtrikman 1962):

$$\sigma_b = \sigma_f + \frac{(1-\phi)}{1/(\sigma_s-\sigma_f) + \phi/3\sigma_f}, \quad (1)$$

where $\phi$ is the fluid fraction, and $\sigma_s$ and $\sigma_f$ are the conductivity of the solid phase and fluid phase, respectively. In the cube model, $\sigma_b$ is expressed as follows:

$$\sigma_b = \left[1-(1-\phi)^{\frac{2}{3}}\right]\sigma_f. \quad (2)$$

Archie's law is also known to address the relationship between $\sigma_b$ and $\phi$ (Archie 1942):

$$\sigma_b = C\phi^m\sigma_f, \quad (3)$$

where $C$ and $m$ are constants. This law is not a geometrical model, but an empirically derived equation (e.g., Watanabe and Kurita 1993; ten Grotenhuis et al. 2005).

We calculated the $\sigma_f$ values from Equations 1 to 3 based on the $\sigma_b$ and $\phi$ determined in the present study at 800 K. The value reported by Yoshino and Noritake (2011) (approximately $3.0 \times 10^{-7}$ S/m) was used as the $\sigma_s$ value in Equation 1. The $m$ value in Equation 3 was assumed as 1. The calculated $\sigma_f$ values at salinities of 3, 5, 10, and 17 wt.% from the three models are summarized in Table 2. Using $\sigma_f$, the relationships between $\sigma_b$ and $\phi$ at the various salinities of 3, 5, 10, and 17 wt.% in the three models were calculated (Figure 5). Figure 5 shows that the three models yield similar values of bulk conductivity. Thus, the value of the fluid fraction needed to realize the high-conductivity anomalies would be similar in the three models. Although the uncertainty in the bulk conductivity arising from the extrapolation from the high fluid fraction (0.19 to 0.30) to the lower fluid fraction would be quite large, we will discuss the salinity and fluid fractions needed to realize the crustal high-conductivity anomalies.

In the case of salinity similar to seawater (3 wt.%), those regions with conductivities of $10^{-3}$ to $10^{-2}$ S/m can be realized by brine-bearing quartzite with a fluid fraction of 0.002 to 0.02. To account for those regions with the highest conductivity of $10^{-1}$ S/m, however, an unrealistically large fluid fraction exceeding 0.2 is required. Thus, an electrical conductivity of $10^{-1}$ S/m is unlikely to be explained by the presence of seawater-like fluids. When salinity is approximately three times higher than that of seawater (10 wt.%), a fluid fraction of 0.04 is required to achieve the conductivity of $10^{-1}$ S/m. Thus, those regions with $10^{-1}$ S/m could be the result of very high salinity fluids. High salinity has been reported in area where evaporite is present (e.g., Yardley and Graham 2002). The Arima-type thermal water originating from the slab-derived fluid is characterized by high salinity (e.g., Masuda et al. 1985). If the salinity is 17 wt.%, those regions with conductivity of $10^{-1}$ S/m could be explained by even smaller fluid fractions of <0.01. Salinities much higher than that of seawater could be achieved by magmatic activity through the formation of a hydrous phase during cooling (e.g., Roedder 1992; De Vivo et al. 1991). Thus, brine-bearing quartzite might account for a large part of the high-conductivity anomalies in regions where fluid has high salinity.

As shown in Figure 4, the conductivity of brine-bearing quartzite is almost independent of temperature, indicating that the conductivity values are sensitive to differences in the salinity and/or fluid fraction rather than changes in temperature. Therefore, although Figure 5 shows the relationship between the bulk conductivity and fluid fraction at 800 K, the constraints of salinity and fluid fraction mentioned above could be applicable at even lower temperatures.

The $\sigma_f$ values estimated from the present results appear to be lower than for both NaCl (Quist and Marshall 1968) and KCl solutions (Nesbitt 1993) with similar salinity (Figure 5). For instance, the $\sigma_f$ with salinity of 3 wt.% is approximately 1.5 orders of magnitude lower than the conductivity of a KCl solution with salinity of 3.6 wt.% at 0.3 GPa reported by Nesbitt (1993) (Figure 5). As the conductivities of the KCl and NaCl solutions rise with pressure (Quist and Marshall 1968), the difference becomes larger at the present experimental pressure of 1 GPa.

**Table 2 $\sigma_f$ with different salinities derived from HS+, cube models, and Archie's law**

| Geometrical model | Salinity of 3 wt.% | Salinity of 5 wt.% | Salinity of 10 wt.% | Salinity of 17 wt.% |
|---|---|---|---|---|
| HS+ model | 0.8 (0.2) | 1.4 (0.1) | 3.8 (0.6) | 20 (3) |
| Cube model | 0.8 (0.2) | 1.4 (0.2) | 4.0 (0.7) | 21 (3) |
| Archie's law[a] | 0.5 (0.1) | 1.0 (0.1) | 2.7 (0.4) | 15 (2) |

Numbers in parentheses represent the uncertainties calculated based on propagation of uncertainties of the fluid fraction and the conductivities ($\sigma_b$, $\sigma_s$). $\sigma_f$, conductivity of fluid. [a]The $m$ value of Archie's law was assumed to be 1.

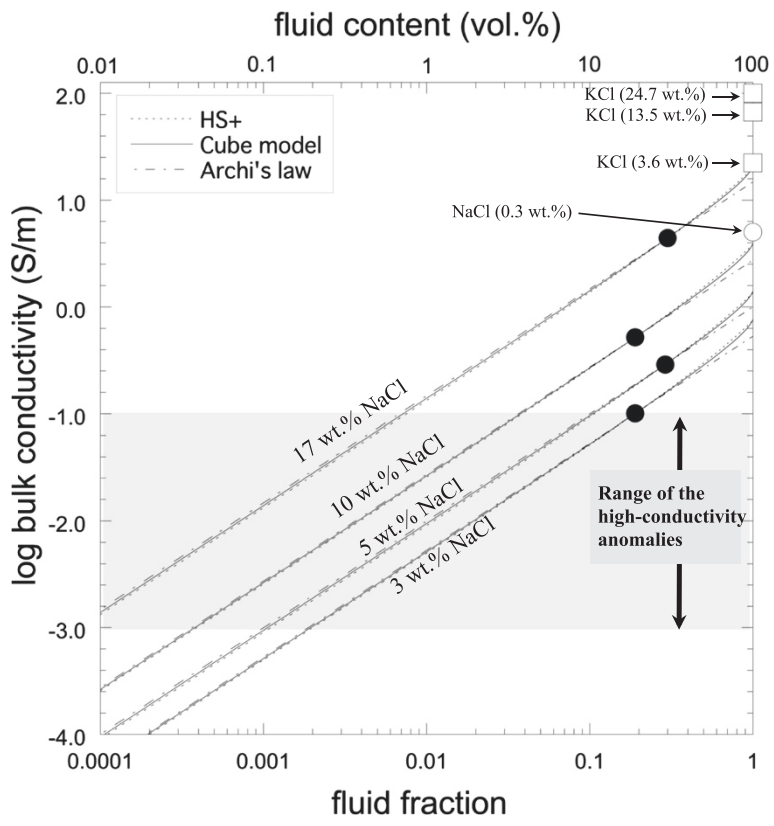


**Figure 5 Bulk conductivity versus fluid fraction at various salinities at 800 K and 1 GPa.** The variables were calculated from the HS + model (dotted lines), cube model (solid lines), and Archie's law (dashed-dotted lines). The solid circles show experimental data points obtained in this study. The open circle and open squares show the conductivities of NaCl with salinity of 0.3 wt.% at 0.4 GPa and 800 K (Quist and Marshall 1968) and KCl with salinities of 3.6, 13.5, and 24.7 wt.% at 0.3 GPa and 773 K (Nesbitt 1993), respectively. The gray region indicates the range of the crustal high-conductivity anomalies ($10^{-3}$ to $10^{-1}$ S/m).

One possible reason for this discrepancy is that a certain amount of $Na^+$ and/or $Cl^-$ could be adsorbed on the surface of the quartz grains, resulting in a decrease in the numbers of charge carriers within the fluid. The adsorption of ionic charge on the quartz surface has been commonly reported in quartz-fluid systems (e.g., Li and De Bruyn 1966). If this effect were large in brine-bearing rocks, performing conductivity measurements on the rock and fluid system would be crucial for evaluating the effects of the fluid fraction on the bulk electrical conductivity. Therefore, using a procedure whereby the bulk electrical conductivity is derived from the electrical conductivities of the rock and solution end-members (e.g., Hyndman and Shearer 1989) could be problematic.

Furthermore, the geometrical distribution of fluid in our samples might not be fully consistent with the HS + and cube models. As shown in Figure 1, some parts of the fluid are present at the grain corners as large pools. This heterogeneous fluid distribution might reduce the effective pathway for the charge carriers (Yoshino et al. 2006). As a result, the $\sigma_f$ values determined in the present study could be lower than might be expected from the HS + and cube models. Based on Figure 5, the bulk conductivities derived from the HS + and cube models are consistent with those from Archie's law with $m \approx 1$ in Equation 3. Because the value of $m$ is commonly around 2 in natural porous rocks (Archie 1942) and because a larger $m$ value leads to a larger $\sigma_f$ value, we calculated the $\sigma_f$ values from Archie's law with $m = 2$ to derive the possible range of reduction of the $\sigma_f$ values. The calculation showed that the $\sigma_f$ values derived from Archie's law with $m = 2$ were about half an order of magnitude larger than those derived from the HS + and cube models. However, the $\sigma_f$ values are still lower than the NaCl (Quist and Marshall 1968) and KCl solutions (Nesbitt 1993), even when considering the half-order-of-magnitude difference. Thus, the effect of the precipitation or absorption of $Na^+$ and/or $Cl^-$ on the mineral surfaces could be a more plausible reason to account for the discrepancies between our $\sigma_f$ values and the NaCl or KCl solutions.

The origin of the conductivity anomalies beneath the Himalayan-Tibetan belt is a widely debated issue (e.g., Gaillard et al. 2004). Recently, Hashim et al. (2013) discussed whether saline fluids could explain the conductivity

anomalies. Based on the salinity of the fluid inclusions in the rocks from this region (25 wt.%) and conductivity data of the KCl solution (Nesbitt 1993), they discussed that a fluid content of approximately 0.8 vol.% was required to explain the values of the conductivity anomalies beneath the Himalayan-Tibetan belt (0.1 to 0.3 S/m). Because this fluid content is essentially lower than the fluid content constrained from the seismic data (at least 10 vol.%), they concluded that the saline fluid hypothesis was not plausible and that the conductivity anomalies beneath the Himalayan-Tibetan belt were better explained by the partially molten rocks. Because their discussion was based on the conductivity data of the KCl solution (Nesbitt 1993) and our $\sigma_f$ values are lower than the KCl solution (Figure 5), we considered whether their conclusion was valid, even if using our $\sigma_f$ values. Although the highest salinity of our data is restricted to 17 wt.%, the required fluid content to explain the values of the conductivity anomalies appears to be approximately 2 vol.%. This fluid content is still lower than the fluid content constrained from the seismic data (at least 10 vol.%). Thus, the saline fluid hypothesis, based on brine-bearing quartzite, might also not be plausible in explaining the conductivity anomalies beneath the Himalayan-Tibetan belt.

In the present study, we used quartzite as a solid analogue phase of fluid-bearing crustal rock. However, Glover and Vine (1994) demonstrated that the conductivity of brine-bearing rocks depends on the rock type. Thus, the conductivity in fluid-bearing rocks could vary according to the presence of other minerals. The lower crust is believed to consist of granulite, gabbro, and amphibolite in which the main constituents are plagioclase, pyroxene, feldspar, and amphibole. Further experiments to investigate the effects of other ionic species, derived from these minerals, on bulk conductivity are needed to constrain more precisely the effects of fluid fraction and salinity.

#### Competing interests
The authors declare that they have no competing interests.

#### Authors' contributions
AS carried out the experimental and analytical works and drafted the manuscript. TY and DY organized the project and helped draft the manuscript. All authors read and approved the final manuscript.

#### Acknowledgements
We thank E. Ito for valuable discussions regarding the manuscript. We also thank the two anonymous reviewers for their constructive comments that have helped us improve the manuscript significantly. This work was supported by a Grant-in-Aid for Scientific Research on Innovative Areas (Research in a Proposed Research Area), 'Geofluids: Nature and Dynamics of Fluids in Subduction Zones' from the Japan Society for Promotion of Science (No. 2109003). AS is supported by the JSPS Research Fellowships for Young Scientists.

Received: 16 October 2013 Accepted: 26 February 2014
Published: 1 April 2014

#### References
Archie GE (1942) Electrical resistivity log as an aid determining some reservoir characters. Trans Am Inst Min Metall Pet Eng 146:54–62
Banks DA, Da Vies GR, Yardley BWD, McCaig AM, Grant NT (1991) The chemistry of brines from an Alpine thrust system in the Central Pyrenees: an application of fluid inclusion analysis to the study of fluid behaviour in orogenesis. Geochim Cosmochim Acta 55:1021–1030
Caricchi L, Gaillard F, Mecklenburgh J, Le Trong E (2011) Experimental determination of electrical conductivity during deformation of melt-bearing olivine aggregates: implications for electrical anisotropy in the oceanic low velocity zone. Earth Planet Sci Lett 302:81–94
De Vivo B, Ayuso RA, Belkin HE, Lima A, Messina A, Viscardi A (1991) Rock chemistry and fluid inclusion studies as exploration tools for ore deposits in the Sila batholith, southern Italy. J Geochem Explor 40:291–310
Duba AG, Shankland TJ (1982) Free carbon and electrical conductivity in the Earth's mantle. Geophys Res Lett 9:1271–1274
Ducea MN, Park SK (2000) Enhanced mantle conductivity from sulfide minerals, southern Sierra Nevada, California. Geophys Res Lett 27:2405–2408
Frost BR, Fyfe WS, Tazaki K, Chan T (1989) Grain-boundary graphite in rocks and implications for high electrical conductivity in the lower crust. Nature 340:134–136
Gaillard F, Scaillet B, Pichavant M (2004) Evidence for present-day leucogranite pluton growth in Tibet. Geology 32:801–804
Glover PWJ, Vine SJ (1994) Electrical conductivity of the continental crust. Geophys Res Lett 21:2357–2360
Hashim L, Gaillard F, Champallier R, Le Breton N, Arbaret L, Scaillet B (2013) Experimental assessment of the relationships between electrical resistivity, crustal melting and strain localization beneath the Himalayan-Tibetan Belt. Earth Planet Sci Lett 373:20–30
Hashin Z, Shtrikman S (1962) A variational approach to the theory of the effective magnetic permeability of multiphase materials. J Appl Phys 33:3125–3131
Hermance JF (1979) The electrical conductivity of materials containing partial melt. Geophys Res Lett 6:613–616
Hyndman RD, Hyndman DW (1968) Water saturation and high electrical conductivity in the lower continental crust. Earth Planet Sci Lett 4:427–432
Hyndman RD, Shearer PM (1989) Water in the lower continental crust: modelling magnetotelluric and seismic reflection results. Geophys J Int 98:343–365
Li HC, De Bruyn PL (1966) Electrokinetic and adsorption studies on quartz. Surf Sci 5:203–220
Marquis G, Hyndman RD (1992) Geophysical support for aqueous fluids in the deep crust: seismic and electrical relationships. Geophys J Int 110:91–105
Masuda H, Sakai H, Chiba H, Matsuhisa Y, Nakamura T (1985) Stable isotopic and mineralogical studies of hydrothermal alteration at Arima Spa, southwest Japan. Geochim Cosmochim Acta 50:19–28
Nesbitt BE (1993) Electrical resistivities of crustal fluids. J Geophys Res 98:4301–4310
Ogawa Y, Mishina M, Goto T, Satoh H, Oshiman N, Kasaya T, Takahashi Y, Nishitani T, Sakanaka S, Uyeshima M, Takahashi Y, Honkura Y, Matsushima M (2001) Magnetotelluric imaging of fluids in intraplate earthquake zones, NE Japan back arc. Geophys Res Lett 28:3741–3744
Olhoeft GR (1981) Electrical properties of granite with implications for the lower crust. J Geophys Res 86:931–936
Ostrovsky IA (1967) On some sources of errors in phase-equilibria investigations at ultra-high pressure; phase diagram of silica. Geol J 5:321–328
Quist AS, Marshall WL (1968) Electrical conductances of aqueous sodium chloride solutions from 0 to 800°C and at pressures to 4000 bars. J Phys Chem 72:684–703
Randles JEB (1947) Kinetics of rapid electrode reactions. Discuss Faraday Soc 1:11–19
Roberts JJ, Tyburczy JA (1999) Partial-melt electrical conductivity: influence of melt composition. J Geophys Res 104:7055–7065
Roedder E (1992) Fluid inclusion evidence for immiscibility in magmatic differentiation. Geochim Cosmochim Acta 56:5–20
Schmeling H (1986) Numerical models on the influence of partial melt on elastic, anelastic and electric properties of rocks. Part II: electrical conductivity. Phys Earth Planet Int 43:123–136
Shimojuku A, Yoshino T, Yamazaki D, Okudaira T (2012) Electrical conductivity of fluid-bearing quartzite under lower crustal conditions. Phys Earth Planet Int 198–199:1–8
Stesky RM, Brace WF (1973) Electrical conductivity of serpentinised rocks to 6 kilobars. J Geophys Res 78:7614–7621
ten Grotenhuis SM, Drury MR, Spiers CJ, Peach CJ (2005) Melt distribution in olivine rocks based on electrical conductivity measurements. J Geophys Res 110, B12201, doi:10.1029/2004JB003462

Waff HS (1974) Theoretical considerations of electrical conductivity in a partially molten mantle and implications for geothermometry. J Geophys Res 79:4003–4010
Wannamaker PE (1986) Electrical conductivity of water-undersaturated crustal melting. J Geophys Res 91:6321–6327
Wannamaker PE, Caldwell TG, Jiracek GR, Maris V, Hill GJ, Ogawa Y, Bibby HM, Bennie SL, Heise W (2009) Fluid and deformation regime of advancing subduction system at Marlborough, New Zealand. Nature 460:733–737
Wasserburg GJ (1958) The solubility of quartz in supercritical water as a function of pressure. J Geol 66:559–578
Watanabe T, Kurita K (1993) The relationship between electrical conductivity and melt fraction in a partially molten simple system. Phys Earth Planet Inter 78:9–17
Watson EB, Brenan JM (1987) Fluids in the lithosphere, 1. Experimentally determined wetting characteristics of $CO_2$-$H_2O$ fluids and their implications for fluid transport, host-rock physical properties, and fluid inclusion formation. Earth Planet Sci Lett 85:171–184
Wood JA Jr (1958) The solubility of quartz in water at high temperatures and pressures. Am J Sci 256:40–47
Yardley BWD, Graham JT (2002) The origins of salinity in metamorphic fluids. Geofluids 2:249–256
Yoshino T (2010) Laboratory electrical conductivity measurement of mantle minerals. Surv Geophys 31:163–206
Yoshino T, Noritake F (2011) Unstable graphite films on grain boundaries in crustal rocks. Earth Planet Sci Lett 306:186–192
Yoshino T, Price DA, Wark DA, Watson EB (2006) Effect of faceting on pore geometry in texturally equilibrated rocks: implications for low permeability at low porosity. Contrib Mineral Petrol 152:169–186
Yoshino T, Lamounier M, McIssac E, Katsura T (2010) Electrical conductivity of basaltic and carbonatite melt-bearing peridotites at high pressures: implications of melt distribution and melt fraction in the upper mantle. Earth Planet Sci Lett 295:593–602

doi:10.1186/1880-5981-66-2
**Cite this article as:** Shimojuku *et al.*: **Electrical conductivity of brine-bearing quartzite at 1 GPa: implications for fluid content and salinity of the crust.** *Earth, Planets and Space* 2014 **66**:2.